Gating Effects for Ion Transport in Three-Dimensional Functionalized Covalent Organic Frameworks

Xiuqin Yu, Cuiyan Li, Jianhong Chang, Yujie Wang, Weifeng Xia, Jinquan Suo, Xinyu Guan, Valentin Valtchev, Yushan Yan, Shilun Qiu, et al.

Covalent Organic Frameworks

DOI: 10.1002/anie.200((will be filled in by the editorial staff))

Gating Effects for Ion Transport in Three-dimensional Functionalized Covalent Organic Frameworks

Xiuqin Yu[†], Cuiyan Li[†], Jianhong Chang, Yujie Wang, Weifeng Xia, Jinquan Suo, Xinyu Guan, Valentin Valtchev, Yushan Yan, Shilun Qiu, and Qianrong Fang**

Abstract: The development of bioinspired nano/subnano-sized (<2 nm) ion channels is still considered a great challenge due to the difficulty in precisely controlling pore's internal structure and chemistry. Herein, for the first time, we report that three-dimensional functionalized covalent organic frameworks (COFs) can act as an effective nanofluidic platform for intelligent modulation of the ion transport. By strategic attachment of 12-crown-4 groups to the monomers as ion-driver door locks, we demonstrate that gating effects of functionalized COFs can be activated by lithium ions. The obtained materials exhibit an outstanding selective ion transmission performance with a high gating ratio (up to 23.6 for JUC-590), which is among the highest values in metal ion-activated solid-state nanochannels reported so far. Furthermore, JUC-590 offers high tunability, selectivity, and recyclability of ion transport proved by the experimental and simulated studies.

Ion channels are omnipresent in biological cells, and they are involved in many intricate processes of transmitting cellular signals by selectively gating ion transport through atomic-scale filters.[1] These natural efficient biological systems inspire researchers to develop artificial counterparts, which could provide widespread applications in energy conversion, ion separation, biosensors, and nanofluidic devices.[2] Gating effects as a basic feature of biological ion channels have been produced by using smart gating functions, which open and close in response to various external stimuli, such as molecules, voltage, pressure, ions, temperature, pH, and light.[3] Among artificial ionic gates, one-dimensional (1D) solid-state nanochannels with different responsive systems have attracted broad attention due to their robustness and durability.[4] However, most of such nanochannels for gating ion transport were very complex and usually prepared by chemical modification with small responsive molecules in huge nanochannels (> 10 nm). This way of preparation makes difficult to precisely control the internal structure and chemistry, and thus usually generates a weak gating effect. Hence, the rational design and synthesis of controllable solid-state nano/subnano-sized (< 2 nm) channels with high gating ratios to mimic the functions of their biological counterparts remains a great challenge.

Covalent organic frameworks (COFs), as a rising class of crystalline porous solid-state materials, are constructed by elaborately integrating organic building units into ordered architectures via covalent bonds.[5] Since the pioneering work of Yaghi and co-workers in 2005,[6] COFs have thrived by virtue of their crystallinity, stability, diverse topologies, and custom-designed pore size and environment. These characteristics endow COF materials with a wide range of applications in gas storage and separation,[7] organic electronics,[8] catalysis,[9] and many others.[10] Especially, three-dimensional (3D) functionalized COFs are considered as a powerful design platform for task-specific uses.[11] For example, Wang et al. prepared two 3D porphyrin-based COFs that are photosensitive and can be used as heterogeneous catalysts for generating singlet oxygen under photoirradiation.[12] Cui and co-workers reported a strategy of incorporating non-enentioselective 1,1′-binaphthol into conformationally rigid pores of 3D COFs, which can induce highly enantioselectivity in the catalytic synthesis of dihydroquinazolinones from aldehydes and anthranilamides.[13] Recently, we have also developed a series of 3D functionalized COFs in view of reticular chemistry, including 3D Salphen-based COFs as catalytic antioxidants,[14] 3D carboxy-functionalized COFs with selective extraction of lanthanide ions,[15] and 3D tetrathiafulvalene-based COFs for tunable electric conductivity.[16] Theoretically, 3D COFs are provided with high specific surface areas, unique pore structures, tailor-made nanospace, and may offer a pathway for ion transport by predesigned, which are of great potentials for an ideal nanofluidic platform to mimic gating mechanisms of biological ion channels. However, such an avenue as a bioinspired ionic gate in COF materials has not been explored yet.

Herein, we report, for the first time, that the 3D crown ether-based COFs, termed JUC-590 and JUC-591 (JUC = Jilin University China), can act as biomimetic nanochannels for efficient gates to regulate ion transport. These functionalized COFs are designed by the incorporation of 12-crown-4 (12C4) groups in the channel walls of COFs based on a bottom-up modification strategy. Owing to the abundant existence of crown ether groups, gating effects of these

[*] X. Yu, C. Li, J. Chang, Y. Wang, W. Xia, J. Suo, X. Guan, Prof. S. Qiu, Prof. Q. Fang
State Key Laboratory of Inorganic Synthesis and Preparative Chemistry,
Jilin University, Changchun 130012, China
E-mail: grfang@jlu.edu.cn or wyujie@jlu.edu.cn
Prof. V. Valtchev
Qingdao Institute of Bioenergy and Bioprocess Technology, Chinese Academy of Sciences
189 Song Ling Rd, Qingdao, Shandong 266101, China
Normandie Univ, ENSICAEN, UNICAEN, CNRS, Laboratoire Catalyse et Spectrochimie, 6 Marechal Juin, 14050 Caen, France
Prof. Y. Yan
Department of Chemical and Biomolecular Engineering, Center for Catalytic Science and Technology, University of Delaware, Newark, DE 19716, USA
[†] These authors contributed equally to this work.

Supporting information for this article is available on the WWW under http://www.angewandte.org or from the author.

Scheme 1. Strategy for preparing 3D functionalized COFs[a]

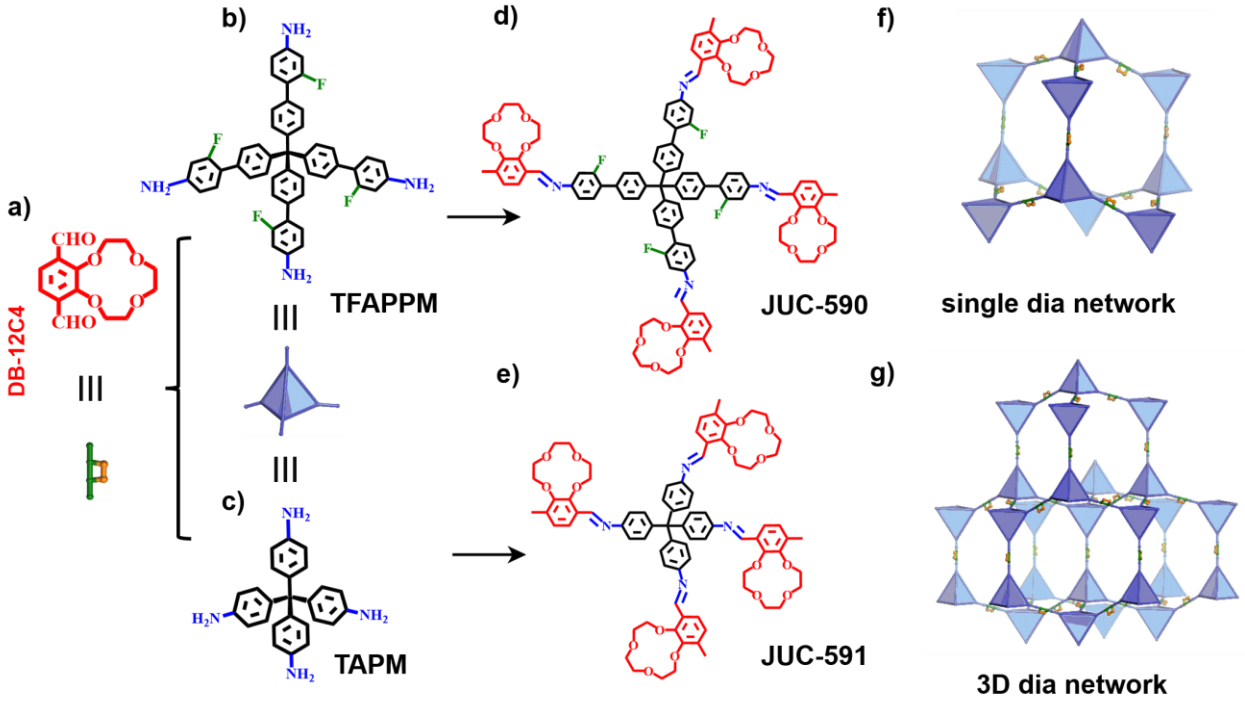

[a]Molecular structures of DB-12C4 as a linear building unit (a) and TFAPPM (b) and TAPM (c) as tetrahedral building units. Two novel 3D COFs, denoted as JUC-590 (d) and JUC-591 (e), constructed by the condensation reaction of DB-12C4 and TFAPPM or TAPM. A single dia network (f) and 3D extended dia structure (g) with decorated edges in these obtained COFs.

obtained COFs can be activated by the lithium ion (Li^+), and thus exhibit an excellent anion traffic performance with a high gating ratio (up to 23.6 for JUC-590), which is among the highest values in all reported metal ion-activated solid-state nanochannels under similar activation conditions. In addition, the experimental and simulated studies reveal the high tunability, selectivity, and recyclability of ion transport in these COF materials. This work thus enables potential new applications of 3D functionalized COFs in the field of the sophisticated biomimetic systems.

To implement this target, we firstly designed a 12C4-modified monomer, 3',6'-dialdehyde benzo-12-crown-4 (DB-12C4, Scheme 1a), as a linear linker. Tetrakis(2-fluoro-4-aminophenyl) phenyl methane (TFAPPM, Scheme 1b), or tetrakis(4-aminophenyl) methane (TAPM, Scheme 1c) was used as a typical tetrahedral building unit. Notably, it is favorable to expand porous structures and surface areas by using tetraphenylmethane-based building blocks, and in particular a series of porous aromatic frameworks (PAFs) with excellent performance have been developed by such tetrahedral nodes.[17] Based on the Schiff-base chemistry, the condensation of DB-12C4 and TFAPPM or TAPM produced two novel 3D functionalized COFs, JUC-590 (Scheme 1d) and JUC-591 (Scheme 1e). With the association of linear linker and tetrahedral nodes, the resulting structures tended to be multifold interpenetrated diamondoid (**dia**) networks with 1D microporous channels (Scheme 1f and 1g).[18] Typically, 3D crown ether-based COFs were prepared by solvothermal reactions of DB-12C4 and TFAPPM or TAPM in a mixture of 1,4-dioxane and mesitylene in the presence of 6 M acetic acid at 120 °C for 3 days.

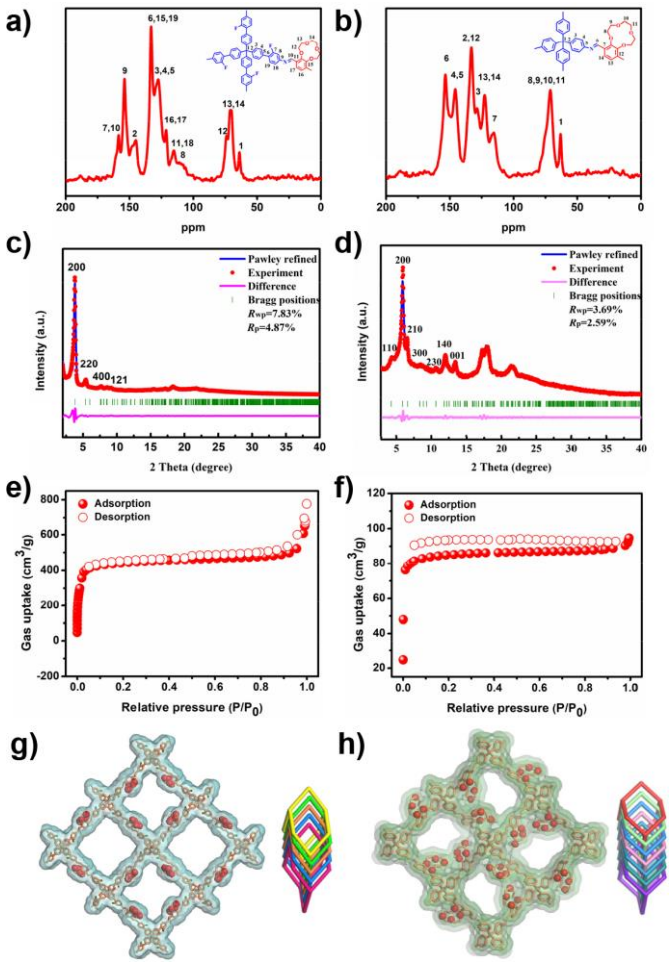

Figure 1. Solid-state ^{13}C CP/MAS NMR spectra of JUC-590 (a) and JUC-591 (b). The experimental and refined PXRD patterns of JUC-590 (c) and JUC-591 (d). N_2 adsorption-desorption isotherms of JUC-590 (e) and JUC-591 (f) at 77 K. Structural representations of JUC-590 (g) and JUC-591 (h).

Multiple characterizations were subsequently employed for their detailed structural definition (Figures S1-S10). Solid-state ^{13}C cross-polarization/magic-angle-spinning (CP/MAS) NMR spectroscopy further confirmed the presence of crown ether moieties in COF backbone after the synthesis (Figure 1a and 1b). The crystalline structures of both COFs were resolved by the powder X-ray diffraction (PXRD) combined with structural simulations (Figure 1c and 1d). Geometrical energy minimization was performed by using Materials Studio software package[19] based on a 5- or 7-fold interpenetrated **dia** net for JUC-590 and JUC-591, respectively. The corresponding unit cell parameters were obtained with $a = b = 46.5811$ Å, $c = 11.9057$ Å and $\alpha = \beta = \gamma = 90°$ for JUC-590 and $a = b = 29.9326$ Å, $c = 6.5676$ Å and $\alpha = \beta = \gamma = 90°$ for JUC-591. The simulated PXRD patterns well matched the experimental results. Full profile pattern matching (Pawley) refinements were carried out on the basis of the experimental data. Peaks at 3.79, 5.41, 7.65, and 8.56° for JUC-590 corresponded to the (200), (220), (400), and (121) Bragg peaks of space group $I4_1$ (No. 80), and peaks at 4.48, 5.95, 6.58, 8.39, 10.65, 12.02, and 13.46° for JUC-591 were ascribed to the (110), (200), (210), (300), (230), (140), and (001) Bragg peaks of space group P-4 (No. 81). The refinement yielded PXRD profiles were almost identical to the experiment ones with good agreement factors (R_{wp} = 7.83% and R_p = 4.87% for JUC-590, R_{wp} = 3.69% and R_p = 2.59% for JUC-591). Alternative structures were also inspected, such as 4- and 6-fold interpenetrated **dia** nets for JUC-590 as well as 6- and 8-fold interpenetrated **dia** nets for JUC-591. However, these simulated PXRD did not match to the experimental ones (Figures S11-S18). According to these results, it is proposed that the obtained 3D COFs have highly interpenetrated **dia** frameworks, 5-fold interpenetration for JUC-590 and 7-fold interpenetration for JUC-591, respectively. The microporous channel of JUC-590 is 1.76 nm and of JUC-591 is 1.02 nm (Figure 1g and 1h). Notably, the tetrahedral tetraphenylmethane-based building units could induce such multi-fold interpenetrated **dia** networks in 3D COFs by interlocking with multiple structures,[11] which is similar with those of other porous materials, such as molecular crystals, metal-organic frameworks (MOFs), and amorphous porous organic materials (POMs).[20]

The permanent porosity and specific surface areas were examined by nitrogen (N_2) adsorption-desorption analysis at 77 K (Figure 1e and 1f). Both functionalized COFs exhibited the typical isotherm of microporous materials with a sharp uptake below 0.05 P/P_0. The slight desorption hysteresis and inclination of isotherms can be attributed to textural mesoporous from the agglomeration of crystals.[21] Based on these adsorption isotherms, Brunauer-Emmett-Teller (BET) surface areas were obtained to be 1521.5 $m^2 g^{-1}$ for JUC-590 and 328.8 $m^2 g^{-1}$ for JUC-591 (Figures S19 and S20). The model of nonlocal density functional theory (NLDFT) was also applied to study the pore size distributions. Both materials showed narrow pore widths with 1.71 nm for JUC-590 and 0.81 nm for JUC-591, respectively (Figures S21 and S22). The lower surface area and smaller pore size of JUC-591 should be caused by its pore shrinkage after the solvent guest removal, which is similar with 3D COFs with the dynamic behavior.[22]

Inspired by the uniform microporous channels and abundant presence of 12C4 groups, we fabricated free-standing Li^+ activated COF-based mixed matrix membranes (MMMs) to study their gating effects for ion transport. It is noted that lithium-regulated nanochannels have promising applications in biosensing, bionic devices, controlled nanofluids, and drug delivery systems.[23] Typically, these membranes, termed JUC-590-MMM and JUC-591-MMM, were prepared by casting poly(ether sulfone) solutions containing the suspended COFs. The obtained translucent membranes displayed good flexibility. The cross-sectional SEM images indicated that the thickness of membranes was ~ 32.0 μm (Figures S23 and S24). Subsequently, the Li^+ activated COF-based MMMs were obtained by immersing them in the aqueous solutions containing diverse concentrations of Li^+.

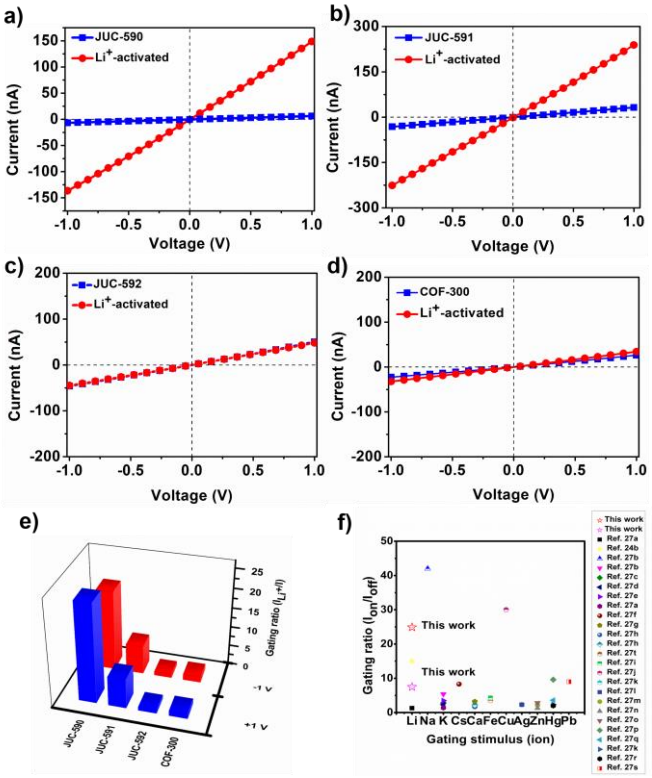

Figure 2. I-V curves of JUC-590-MMM (a), JUC-591-MMM (b), JUC-592-MMM (c), and COF-300-MMM (d) before (blue square) and after (red circle) activation with Li^+. (e) The gating ratio (I_{Li}^+/I) of JUC-590-, JUC-591-, JUC-592- and COF-300-MMM at -1 V and +1 V. (f) Comparison of the gating ratios of 3D functionalized COFs and other reported 1D nanochannels activated by metal ions.

The gating properties of COFs were demonstrated by the transmembrane ion current, which was monitored by using a home-made electrochemical device (Figure S25). The current-voltage (I-V) curves before and after Li^+ activation were recorded in the presence of 0.1 M Tris-HCl buffer (pH = 7.56) as the electrolyte. As shown in Figure 2, low ion current from inactive COF-based MMMs manifests that the nanochannels were in the ″close″ state. However, when the nanochannels of JUC-590-MMM were activated by Li^+ (10 μM), the current through the membrane increased from 6.3 nA to 148.7 nA at +1 V and -6.7 nA to -136.7 nA at -1 V, suggesting that the channel gating changed from ″close″ to ″open″ state (Figure 2a). These results can be attributed to the change of charges in the wall of COFs from neutral to positive, generating from the binding of Li^+ with 12C4.[24]

Similarly, after JUC-591-MMM was activated by Li^+ (1 μM), its ionic current through the nanochannels increased from 32.2 nA to 238.6 nA at +1 V and -31.4 nA to -225.7 nA at -1 V (Figure 2b). As a comparison, we synthesized two 3D COFs without the crown ether group, COF-300 and JUC-592.[25] Various characterizations were carried out to determine the detailed structure of JUC-592 (Figures S26-S33). As predicted, there were no obvious changes in I-V curves before and after Li^+ activation of JUC-592- and COF-300-based MMMs (Figure 2c and 2d).

To further evaluate ion-gated properties of the nanochannels of COFs, the gating ratio (I_{Li^+}/I), defined as the ratio of transmembrane current after activation with Li^+ (I_{Li^+}) to the initial current (I), was provided. Remarkably, the gating ratios showed a striking difference between crown ether-based and free COFs (Figure 2e). The gating ratios were ~ 1.0 at ±1 V for both unfunctionalized COF-based MMMs (JUC-592 and COF-300), while crown ether-based COFs had much higher gating ratios, 23.6 at +1 V and 20.4 at –1 V for JUC-590-MMM and 7.4 at +1 V and 7.2 at –1 V for JUC-591-MMM, which is one order of magnitude higher than those of unfunctionalized COFs. We also summarized the gating ratios of metal ion activated solid nanochannels reported so far in Figure 2f and Table S1.[23b,26] Notably, the gating ratio of JUC-590-MMM (23.6) surpassed almost all reported values of 1D nanochannels under similar activation conditions, such as SsDNA-Alumina (2.3),[26k] 4-AB18C6-PI (5.4),[26b] and HDA–MAP5-PET (9.6).[26p]

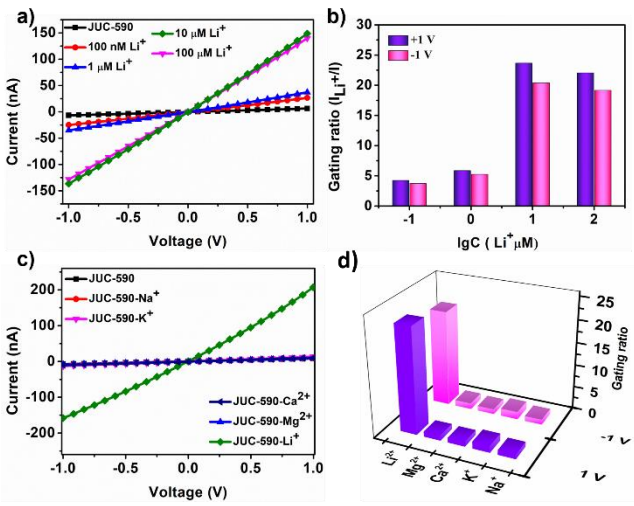

Figure 3. (a) The I-V curves of JUC-590-MMM before and after activation with different concentrations of Li^+. (b) The concentration-dependent changes of gating ratio (I_{Li^+}/I) of JUC-590-MMM at -1 V and +1 V. (c) I-V curves of JUC-590-MMM after activation with different metal ions at -1 V and +1 V. (d) The gating ratios of JUC-590-MMM after activation with different metal ions at -1 V and +1 V.

In order to confirm the tunability of 3D functionalized COFs in gating ion transport, the I-V curves were recorded after activation with different concentrations of Li^+. Before activation with Li^+, the current of JUC-590-MMM was about 6.3 nA at +1 V and -6.7 nA at -1 V. As the concentration of Li^+ increased from 0.1 μM to 10 μM, the current of JUC-590-MMM was improved from 26.7 nA to 148.7 nA at +1 V and from -25.0 nA to -136.7 nA at -1 V, with the gating ratio changing from 4.2 to 23.6 at +1 V and from 3.7 to 20.4 at -1 V (Figure 3a and 3b). When the concentration of Li^+ was further increased to 100 μM, the current and gating ratio of JUC-590-MMM showed a slight drop (Figure S34). Similarly, the current of JUC-591-MMM is about 32.2 nA at +1 V and -31.4 nA at -1 V before activation with Li^+, and subsequently the current was increased from 82.4 nA to 238.6 nA at +1 V and from -75.5 nA to -225.7 nA at -1 V with the varied concentration of Li^+ from 0.1 μM to 1 μM. The gating ratios augmented from 2.6 to 7.4 at +1 V and from 2.4 to 7.2 at -1 V, respectively. However, as the Li^+ concentration further enlarged to 10 μM, its current decreased to 150.3 nA at +1 V and -126.7 nA at -1 V, and the gating ratios dropped to 4.7 at +1 V and 4.0 at -1 V (Figures S35-S37). The variation of transmembrane current could be associated with the changes in the surface charge and wettability of materials.[27] Consequently, we tested the water contact angles of COF-based MMMs. As shown in Figure S38, the mean water contact angles of inactive samples were 85.5 ± 1.6° for JUC-590-MMM and 86.9 ± 5.4° for JUC-591-MMM. After being activated by Li^+, their water contact angles were increased to 105.0 ± 2.1° and 100.6 ± 0.9°, respectively. Clearly, the positive charge of COF-based MMMs gradually increased with the concentration of Li^+, thus enhancing the transmembrane current. Simultaneously, as the Li^+ concentration further increased, the wettability could play a prominent role in the changing of current, which causes a drop in current.

The specific selectivity of the ionic gate is important for biological ion channels to perform essential functions. The selectivity of JUC-590-MMM was evaluated by using different alkali and alkaline earth metal ions, including Li^+, Na^+, K^+, Ca^{2+} and Mg^{2+}. Notably, unlike the Li+-activated phenomenon, no obvious differences in I-V curves were found before and after JUC-590-MMM was activated by Na^+, K^+, Ca^{2+}, and Mg^{2+}, which demonstrates almost no interaction or complexation of these cations with 12C4 (Figure 3c). Since the 12C4 possessed a cavity radius of 1.2-1.5 Å, only the Li^+ with a small radius of 1.2 Å was comparable to the cavity size (Figure S39). Accordingly, after treatment with different cations, the gating ratios were 1.1 for Na^+, 1.6 for K^+, 1.1 for Ca^{2+}, and 1.2 for Mg^{2+} at +1 V as well as 1.2 for Na^+, 1.7 for K^+, 1.1 for Ca^{2+}, and 1.3 Mg^{2+} at -1 V, respectively, which are much lower than those of Li^+-activated samples (Figure 3d). Also, we examined the responsive switchability of COF-based ionic gates. As ethylenediaminetetraacetic acid (EDTA) has a strong chelating ability to form complexes with metal ions, JUC-590-MMM can achieve reversible switching upon alternatively immersing in Li^+ and EDTA aqueous solutions. The current of Li^+-activated JUC-590-MMM was 178.1 nA at +1 V and -149.9 nA at -1 V, indicating the gate is in an ″open″ state. After soaking in EDTA aqueous solution, its current decreased to 12.4 nA at +1 V and -11.1 nA at -1 V, respectively, which demonstrates that the gate is in a "close" state. The reversible switching of JUC-590-MMM can be performed repeatedly at least three times without obvious change of the ionic current (Figure S40).

Furthermore, reversal potential (Vr) measurements were carried out, in which two reservoirs were filled with different concentrations of KCl (Figure 4a). After activation with Li^+, positive Vr was obtained as 40.2 mV for JUC-590-MMM and 46.3 mV for JUC-591-MMM, respectively (Figure 4b and 4c). These positive values indicated that anion-selective nanochannels were predominant in Li^+-activated COFs. The permeability ratios were acquired based on the Goldman-Hodgkin-Katz equation as follows (Eq.1).[28]

$$\frac{P_{Cl^-}}{P_{K^+}} = \frac{a_{K^+,HC} - a_{K^+,LC} \cdot \exp\left(-\frac{V_r F}{RT}\right)}{a_{Cl^-,HC} \cdot \exp\left(-\frac{V_r F}{RT}\right) - a_{Cl^-,LC}} \quad (1)$$

Thus, the Cl^-/K^+ permeability ratios were calculated to be 9.8 for JUC-590-MMM (15.3 for JUC-591-MMM) after activation with Li^+ (Figure 4d). These results indicated that the binding of Li^+ with 12C4 could generate an ionic nanochannel with fixed cationic sites, which leads to highly selective anion transport. Furthermore, MD simulations for JUC-590 were also performed.[28b] The layer of JUC-590 was sandwiched between KCl aqueous solution and deionized water. Starting from a random configuration, followed by a 1 fs production run, the system was stopped after a run of 1 ns. The schematic diagram of the system showed that only Cl^- ions could transport from the KCl aqueous solution to deionized water through the COF layer at certain intervals, which demonstrates a higher transport activity of anions than that of cations via Li^+-activated JUC-590 (Figures 4e and S41).

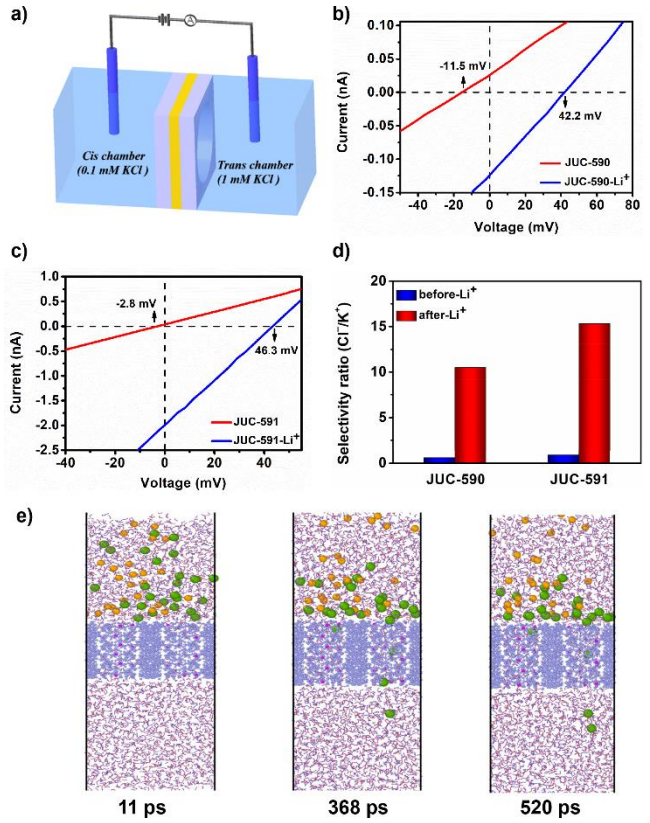

Figure 4. (a) Schematic illustration of the set-up for ions transport with asymmetric bulk electrolyte concentrations. (b) Asymmetric I-V curves for JUC-590-MMM before and after activation with Li^+ under a 10-fold salinity gradient. (c) Asymmetric I-V curves for JUC-591-MMM before and after activation with Li^+ under a 10-fold salinity gradient. (d) ion selectivity ratios (Cl^-/K^+) of JUC-590-MMM and JUC-591-MMM before and after activation with Li^+. (e) The schematic diagram of ion transport behavior through JUC-590.

In order to explore the actual applications of 3D functionalized COFs, we further investigated the osmotic energy conversion of JUC-590-MMM and JUC-591-MMM (Figure S42 and Supplementary Section 1). The energy conversion is evaluated by collecting I-V scans under a series of transmembrane concentration gradients. The corresponding short-circuit current (I_{sc}) and open-circuit voltage (V_{oc}) were obtained from the intercepts on the current and voltage axes (Figures 5a and S43). The maximum output power (P_{max}), calculated by the equation of $P_{max} = V_{oc} \times I_{sc}/4$, is 0.13 nW for JUC-590-MMM and 0.19 nW for JUC-591-MMM at a concentration gradient of 5000 (Figures S44 and S45).[29a] The harvested power can be exported by supplying an external load resistor (R_L, Figure S46), calculated as $P_{out} = I^2 \times R_L$.[29b] As shown in Figures 5b and S47, the current density on the external circuit decreased as the load resistance increased. When the external resistance was ~1000 kΩ for JUC-590-MMM and ~100 kΩ for JUC-591-MMM, their maximum power densities were 0.18 mW/m^2 and 0.17 mW/m^2, respectively (Figures 5c, 5d, S48, and S49).

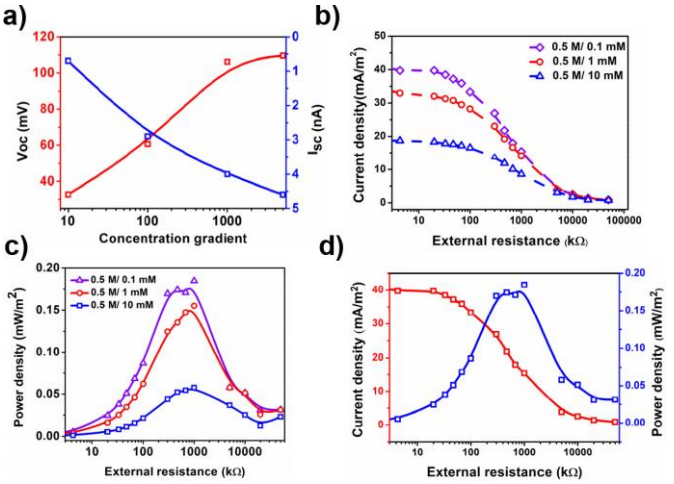

Figure 5. (a) The V_{oc} and I_{sc} of JUC-590-MMM under various concentration gradients. (b) Current density of JUC-590-MMM as functions of load resistance under various concentration gradients. (c) Power output of JUC-590-MMM as functions of load resistance under various concentration gradients. (d) Corresponding current density and power density of JUC-590-MMM under different external resistances and a 5000-fold salinity gradient (C_H/C_L = 0.5 M/0.1 mM).

In summary, we have developed two 3D crown ether-containing COFs with 1D nanochannels, JUC-590 and JUC-591, in which 12C4 groups are attached in the channel walls based on a bottom-up synthetic strategy. Due to 1D nanoscale channels, large surface area, and high density of 12C4 groups, these 3D functionalized COFs can be activated by Li^+ ions and be utilized as a nanofluidic platform to control ion transport and achieve the potential for harvesting osmotic energy generation. Remarkably, these materials exhibited a close-to-open switching of the nanochannels with excellent gating ratios (as high as 23.6 for JUC-590), which is among the highest values of reported metal ion-activated 1D nanochannels. Moreover, JUC-590 also showed the high tunability, selectivity, and recyclability of ion transport unambiguously proved by the experimental and modeling studies. This work thus opens a new pathway to design 3D functionalized COFs as smart artificial nanochannel materials to gain the promising features of sophisticated biological systems.

Acknowledgments

This work was supported by National Natural Science Foundation of China (22025504, 21621001, and 21390394), ″111″ project (BP0719036 and B17020), China Postdoctoral Science Foundation (2020TQ0118 and 2020M681034), and the program for JLU Science and Technology Innovative Research Team. V.V., Q.F. and S.Q. acknowledge the collaboration in the framework of China-French joint laboratory "Zeolites".

Conflict of interest

The authors declare no conflict of interest.

Received: ((will be filled in by the editorial staff))
Published online on ((will be filled in by the editorial staff))

Keywords: covalent organic frameworks, functionalization, ion channels, gating effect

[1] M. Tagliazucchi, I. Szleifer, *Mater. Today* **2015**, *18*, 131-142.

[2] a) Z. Zhang, L. P. Wen, L. Jiang, *Chem. Soc. Rev.* **2018**, *47*, 322-356; b) X. J. Jiang, L. Wang, S. D. Liu, F. Li, J. Q. Liu, *Mater. Chem. Front.* **2021**, *5*, 1610-1631.

[3] Z. Zhang, X. D. Huang, Y. C. Qian, W. P. Chen, L. P. Wen, L. Jiang, *Adv. Mater.* **2019**, *32*, 1904351.

[4] a) D. F. Ding, P. C. Gao, Q. Ma, D. G. Wang, F. Xia, *Small* **2019**, *15*, 1804878; b) K. Xiao, L. P. Wen, L. Jiang, *Small* **2016**, *12*, 2810-2831.

[5] R. Y. Liu, K. T. Tan, Y. F. Gong, Y. Z. Chen, Z. E. Li, S. L. Xie, T. He, Z. Lu, H. Yang, D. L. Jiang, *Chem. Soc. Rev*. **2020**, *50*, 120-242.

[6] A. P. Côté, A. I. Benin, N. W. Ockwig, M. O'Keeffe, A. J. Matzger, O. M. Yaghi, *Science* **2005**, *310*, 1166-1170.

[7] a) S. S. Han, H. Furukawa, O. M. Yaghi, W. A. Goddard III, *J. Am. Chem. Soc.* **2008**, *130*, 11580-11581; b) X. Y. Guan, Y. C. Ma, H. Li, Y. Yusran, M. Xue, Q. R. Fang, Y. S. Yan, V. Valtchev, S. L. Qiu, *J. Am. Chem. Soc.* **2018**, *140*, 4494-4498.

[8] a) S. Wan, J. Guo, J. Kim, H. Ihee, D. Jiang, *Angew. Chem. Int. Ed.* **2008**, *47*, 8826-8830; *Angew. Chem*. **2009**, *121*, 3253-3253; b) S. Y. Ding, J. Gao, Q. Wang, Y. Zhang, W. G. Song, C. Y. Su, W. Wang, *J. Am. Chem. Soc*. **2011**, *133*, 19816-19822.

[9] a) Q. R. Fang, S. Gu, J. Zheng, Z. B. Zhuang, S. L. Qiu, Y. S. Yan, 3 *Angew. Chem. Int. Ed*. **2014**, *53*, 2878-2882; *Angew. Chem.* **2014**, *126*, 2922-2926; b) H. Li, Q. Y. Pan, Y. C. Ma, X. Y. Guan, M. Xue, Q. R. Fang, Y. S. Yan, V. Valtchev, S. L. Qiu, *J. Am. Chem. Soc.* **2016**, *138*, 14783-14788.

[10] a) Q. R. Fang, Z. B. Zhuang, S. Gu, R. B. Kaspar, J. Zheng, J. H. Wang, S. L. Qiu, Y. S. Yan, *Nat. Commun*. **2014**, *5*, 4503-4511; b) T. Y. Zhou, S. Q. Xu, Q. Wen, Z. F. Pang, X. Zhao, *J. Am. Chem. Soc*. **2014**, *136*, 15885-15888; c) Z. L. Li, H. Li, X. Y. Guan, J. J. Tang, Y. Yusran, Z. Li, M. Xue, Q. R. Fang, Y. S. Yan, V. Valtchev, S. L. Qiu, *J. Am. Chem. Soc*. **2017**, *139*, 17771-17774; d) Y. Y. Zhang, J. Y. Duan, D. Ma, P. F. Li, S. W. Li, H. W. Li, J. W. Zhou, X. J. Ma, X. Feng, B. Wang, *Angew. Chem. Int. Ed.* **2017**, *56*, 16313-16317; *Angew. Chem*. **2017**, *129*, 16531-16535.

[11] X. Y. Guan, F. Q. Chen, Q. R. Fang, S. L. Qiu, *Chem. Soc. Rev*. **2020**, *49*, 1357-1384.

[12] G, Q. Lin, H, M. Ding, R. F. Chen, Z. K. Peng, B. S. Wang, C. Wang, *J. Am. Chem. Soc.* **2017**, *139*, 8705-8709.

[13] B. Hou, S. Yang, K. W. Yang, X. Han, X. H. Tang, Y. Liu, J. W. Jiang, Y. Cui, *Angew. Chem. Int. Ed.* **2021**, *60*, 6086-6093; *Angew. Chem.* **2021**, *133*, 6151-6158.

[14] S. C. Yan, X. Y. Guan, H. Li, D. H. Li, M. Xue, Y. S. Yan, V. Valtchev, S. L. Qiu, Q. R. Fang, *J. Am. Chem. Soc.* **2019**, *141*, 2920-2924.

[15] Q. Y. Lu, Y. C. Ma, H. Li, X. Y. Guan, Y. Yusran, M. Xue, Q. R. Fang, Y. S. Yan, S. L. Qiu, V. Valtchev, *Angew. Chem. Int. Ed*. **2018**, *57*, 6042-6048; *Angew. Chem*. **2018**, *130*, 6150-6156.

[16] H. Li, J. H. Chang, S. S. Li, X. Y. Guan, D. H. Li, C. Y. Li, L. X. Tang, M. Xue, Y. S. Yan, V. Valtchev, S. L. Qiu, Q. R. Fang, *J. Am. Chem. Soc*. **2019**, *41*, 13324-13329.

[17] a) T. Ben, H. Ren, S. Q. Ma, D. P. Cao, J. H. Lan, X. F. Jing, W. C. Wang, J. Xu, F. Deng, J. M. Simmons, S. L. Qiu, G. S. Zhu, *Angew. Chem. Int. Ed*. **2009**, *48*, 9457-9460; *Angew. Chem.* **2009**, *121*, 9621-9624; b) A. Comotti, S. Bracco, T. Ben, S. Qiu, P. Sozzani, *Angew. Chem. Int. Ed*. **2014**, *53*, 1043-1047; *Angew. Chem.* **2014**, *126*, 1061-1065; c) G. Xing, I. Bassanetti, S. Bracco, M. Negroni, C. Bezuidenhout, T. Ben, P. Sozzani, A. Comotti, *Chem Sci.* **2019**, *10*, 730-736; d) J. Perego, S. Bracco, A. Comotti, D. Piga, I. Bassanetti, P. Sozzani, Angew. Chem. Int. Ed. **2021**, *60*, 6117-6123; *Angew. Chem.* **2021**. *133*, 6182-6188; e) J. Perego, D. Piga, S. Bracco, P. Sozzani, A. Comotti, *Chem Comm.* **2018**, *54*, 9321-9324; f) I. Bassanetti, S. Bracco, A. Comotti, M. Negroni, C. Bezuidenhout, S. Canossa, P. P. Mazzeo, L. Marchio, P. Sozzani, *J. Mater. Chem. A*. **2018**, *6*, 14231-14239.

[18] C. Bonneau, O. Delgado-Friedrichs, M. O'Keeffe, O. M. Yaghi, Acta *Crystallogr*. **2004**, *A60*, 517-520.

[19] Materials Studio ver. 7.0, Accelrys Inc., San Diego, CA.

[20] a) J. F. Uribe-Romo, J. R. Hunt, H. Furukawa, C. Klöck, M. O′Keeffe, O. M. Yaghi, *J. Am. Chem. Soc*. **2009**, 131, 4570-4571; b) V. A. Blatov, L. Carlucci, G. Ciani, D. M. Proserpio, *Cryst. Eng. Comm.* **2004**, *6*, 377-395; c) C. Bonneau, O. D. F, M. O, Yaghi, O. M. *Acta Crystallogr. A* **2004**, *60*, 517-520; d) W. Guo, E. Galoppini, R. Gilardi, G. I. Rydja, Y. H. Chen, *Cryst. Growth Des*. **2001**, *1*, 231-237; e) O. Plietzsch, C. I. Schilling, M. Tolev, M. Nieger, C. Richert, T. Muller, S. Brase, *Org. Biomol. Chem.* **2009**, *7*, 4734–4743.

[21] Q. R. Fang, J. H. Wang, S. Gu, R. B. Kaspar, Z. B. Zhuang, J. Zheng, H. X. Guo, S. L. Qiu, Y. S. Yan, *J. Am. Chem. Soc.* **2015**, *137*, 8352-8355.

[22] a) Y. X. Ma, Z. J. Li, L. Wei, S. Y. Ding, Y. B. Zhang, W. Wang, *J. Am. Chem. Soc.* **2017**, *139*, 4995-4998; b) Y. J. Wang, Y. Z. Liu, H. Li, X. Y. Guan, M. X, Y. Yan, V. Valtchev, S. L. Qiu, and Q. R. Fang, *J. Am. Chem. Soc*. **2020**, *142*, 3736–3741.

[23] a) R. J. Baldessarini, L. Tondo, P. Davis, M. Pompili, F. K. Goodwin, J. Hennen, *Bipolar Disord.* **2006**, *8*, 625-639. b) M. Ali, I. Ahmed, P. Ramirez, S. Nasir, S. Mafe, C. M. Niemeyer, W. Ensinger, *Anal. Chem.* **2018**, *90*, 6820-6826.

[24] H. Daiguji, P. D. Yang, A. Majumdar, *Nano Letters*. **2004**, *39*, 137-142.

[25] F. J. Uribe-Romo, J. R. Hunt, H. Furukawa, C. Klöck, M. O'Keeffe, O. M. Yaghi, *J. Am. Chem. Soc*. **2009**, *131*, 4570-4571.

[26] a) X. Hou, W. Guo, F. Xia, F. Q. Nie, H. Dong, Y. Tian, L. P. Wen, L. Wang, L. X. Cao, Y. Yang, J. M. Xue, Y. L. Song, Y. G. Wang, D. S. Liu, L. Jiang, *J. Am. Chem. Soc.* **2009**, *131*, 7800-7805; b) Q. Liu, K. Xiao, L. P. Wen, H. Lu, Y. H. Liu, X. Y. Kong, G. H. Xie, Z. Zhang, Z. S. Bo, L. Jiang, *J. Am. Chem. Soc*. **2015**, *137*, 11976-11983; c) Y. F. Wu, D. Y. Wang, I. Willner, Y. Tian, L. Jiang, *Angew. Chem. Int. Ed.* **2018**, *57*, 7790-7794; *Angew. Chem*. **2018**, *130*, 7916-7920; d) M. Y. Liu, H. C. Zhang, K. Li, L. P. Heng, S. T. Wang, Y. Tian, L. Jiang, *Adv. Funct. Mater.* **2015**, *25*, 421-426; e) K. Wu, K. Xiao, L. Chen, R. Zhou, B. Niu, Y. Q. Zhang, L. P. Wen, *Langmuir* **2017**, *33*, 8463-8467; f) M. Ali, I. Ahmed, P. Ramirez, S. Nasir, J. Cervera, S. Mafe, C. M. Niemeyer, W. Ensinger, *Langmuir* **2017**, *33*, 9170-9177; g) M. Ali, S. Nasir, P. Ramirez, J. Cervera, S. Mafe, W. Ensinger, *ACS. Nano.* **2012**, *6*, 9247-9257; h) Z. Meng, C. D. Jiang, X. L. Li, J. Zhai, *ACS Appl. Mater. Interfaces.* **2014**, *6*, 3794-3798; i) C. Zhao, X. S. Li, L. Y. Li, X. Gong, Y. Chang, J. Zheng, *Chem. Commun.* **2013**, *49*, 9317-9319; j) Y. Chen, D. Zhou, Z. Y. Meng, J. Zhai, *Chem. Commun.* **2016**, *52*, 10020-10023; k) H. M. Wang, S. N. Hou, Q. Q. Wang, Z. W. Wang, X. Fan, J. Zhai, *J. Mater. Chem. B.* **2015**, *3*, 1699-1705; l) L. J. Gao, P. Li, Y. Q. Zhang, K. Xiao, J. Ma, G. H. Xie, G. L. Hou, Z. Zhang, L. P. Wen, L. Jiang, *Small* **2014**, *11*, 543-547; m) C. P. Han, H. Y. Su, Z. Y. Sun, L. Wen, D. M. Tian, K. Xu, J. F. Hu, A. Wang, H. B. Li, L. Jiang, *Chem. Eur. J.* **2013**, *19*, 9388-9395; n) Y. Tian, X. Hou, L. P. Wen, W. Guo, Y. L. Song, H. Z. Sun, Y. G. Wang, L. Jiang, D. B. Zhua, *Chem.Commun.* **2010**, *46*, 1682-1684; o) Y. Sun, F. Zhang, Z. Y. Sun, M. M. Song, D. M. Tian, H. B. Li, *Chem. Eur. J.* **2016**, *22*, 4355-4358; p) F. Zhang, J. K. Ma, Y. Sun, I. Boussouar, D. Tian, H. B. Li, L. Jiang, *Chem. Sci.* **2016**, *7*, 3227-3233; q) Y. Tian, Z. Zhang, L. P. Wen, J. Ma, Y. Q. Zhang, W. D. Liu, J. Zhai, L. Jiang, *Chem. Commun.* **2013**, *49*, 10679-10681; r) L. Shi, F. J. Jia, L. Wang, M. Jalalah, M. S. Al-Assirib, T. Gao, Farid A. Harrazb, G. Li, *Sens. Actuators B Chem.* **2021**, *326*, 128976; s) Y. C. Qian, Z. Zhang, W. Tian, L. P. Wen, L. Jiang, *Faraday Discuss.* **2018**, *210*, 101-111; t) B. Niu, K. Xiao, X. D. Huang, Z. Zhang, X. Y. Kong, Z. Q. Wang, L. P. Wen, L. Jiang, *ACS Appl. Mater. Interfaces.* **2018**, *10*, 22632-22639.

[27] X. Q. Zhang, H. L. Liu, L. Jiang, *Adv. Mater.* **2018**, *31*, 1804508.

[28] a) S. Chen, C. J. Zhu, W. P. Xian, X. Y. Liu, X. L. Liu, Q. H. Zhang, S. Q. Ma, Q. Sun, *J. Am. Chem. Soc.* **2021**, *143*, 9415-9422; b) P. C. Zhang, S. F. Chen, C. J. Zhu, L. X. Hou, W. P. Xian, X. H. Zuo, Q. H. Zhang, L. Zhang, S. Q. Ma, Q. Sun, *Nat. Commun.* **2021**, *12*, 1844-1851.

[29] a) J. Z. Ji, Q. Kang, Y. Zhou, Y. P. Feng, X. Chen, J. Y. Yuan, W. Guo, Y Wei, L. Jiang, *Adv. Funct. Mater.* **2016**, *27*, 1603623; b) F. Yan, L. Yao, K. X. Chen, Q. Y, B. Su, *J. Mater. Chem. A*, **2019**, *7*, 2385-2391.

Covalent Organic Frameworks

*Xiuqin Yu, Jianhong Chang, Yujie Wang, Weifeng Xia, Jinquan Suo, Xinyu Guan, Valentin Valtchev, Yushan Yan, Shilun Qiu, and Qianrong Fang**

_____ *Page – Page*

Gating Effects for Ion Transport in Three-dimensional Functionalized Covalent Organic Frameworks

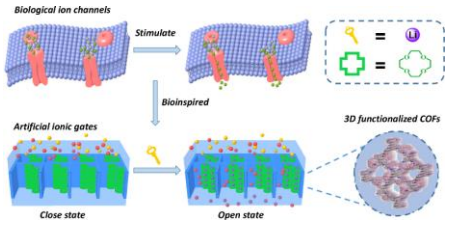

Herein, we firstly report that the crown ether-functionalized 3D COFs can efficiently gate ion transport with an excellent gating ratio up to 23.6, which is among the highest values in metal ion-activated solid-state nanochannels reported so far.